

Slack K⁺ channels limit kainic acid-induced seizure severity in mice by modulating neuronal excitability and firing

David Skrabak¹, Helmut Bischof¹, Thomas Pham¹, Peter Ruth¹, Rebekka Ehinger¹, Lucas Matt^{1,2} & Robert Lukowski^{1,2}  

Mutations of the Na⁺-activated K⁺ channel Slack (KCNT1) are associated with terrible epilepsy syndromes that already begin in infancy. Here we report increased severity of acute kainic acid-induced seizures in adult and juvenile Slack knockout mice (Slack^{-/-}) *in vivo*. Fittingly, we find exacerbation of cell death following kainic acid exposure in organotypic hippocampal slices as well as dissociated hippocampal cultures from Slack^{-/-} *in vitro*. Furthermore, in cultured Slack^{-/-} neurons, kainic acid-triggered Ca²⁺ influx and K⁺ efflux as well as depolarization-induced tetrodotoxin-sensitive inward currents are higher compared to the respective controls. This apparent changes in ion homeostasis could possibly explain altered action potential kinetics of Slack^{-/-} neurons: steeper rise slope, decreased threshold, and duration of afterhyperpolarization, which ultimately lead to higher action potential frequencies during kainic acid application or injection of depolarizing currents. Based on our data, we propose Slack as crucial gatekeeper of neuronal excitability to acutely limit seizure severity.

¹ Department of Pharmacology, Toxicology and Clinical Pharmacy, Institute of Pharmacy, University of Tübingen, Tübingen, Germany. ²These authors contributed equally: Lucas Matt, Robert Lukowski.  email: robert.lukowski@uni-tuebingen.de

The sodium ion (Na^+)-activated potassium ion (K^+) channel Slack (sequence like a calcium ion (Ca^{2+})-activated K^+ channel, $\text{K}_{\text{Na}1.1}$, Slo2.2) is predominantly expressed in central and peripheral neurons^{1–4}. Due to its high conductance, Slack effectively regulates neuronal excitability by limiting action potential (AP) frequency^{5–8}, increasing afterhyperpolarization (aHP)^{9,10}, and setting the resting membrane potential (RMP)^{11–14}. As Slack channels are gated by high intracellular Na^+ concentrations ($[\text{Na}^+]$) of ~40 mmol/l^{15,16}, they are thought to activate under physiological conditions by forming functional micro-domains with Na^+ sources. Respective physical or functional interactions of Slack were demonstrated with voltage-activated Na^+ channels¹⁷, α -amino-3-hydroxy-5-methyl-4-isoxazole propionic acid (AMPA)-^{18–20} and N-methyl-D-aspartate (NMDA)-type glutamate receptors^{21,22}.

Mutations of the Slack gene *KCNT1* are linked to at least two devastating childhood epilepsy syndromes that are, so far, mostly intractable by common antiepileptic drugs^{23,24}. *Epilepsy of Infancy with Migrating Focal Seizures* (EIMFS) shows onset in the first weeks of life leading to severe developmental delay²⁵ while *Autosomal Dominant Nocturnal Frontal Lobe Epilepsy* (ADNFLE) is a serious non-rapid eye movement (REM) sleep-related frontal lobe epilepsy with onset at an age of approximately 5 years^{24–27}. Currently described disease-causing mutations are predominantly gain of function (GOF) mutations, that increase K^+ conductance, open probability, Na^+ sensitivity, or inter-subunit cooperativity, with the latter resulting in intermediate conductance states^{28–30}. Interestingly, also a loss of function (LOF) variant of Slack was described to cause severe early infantile epilepsy^{31,32}, while increased susceptibility to glutamate excitotoxicity was recently reported for global Slack^{−/−} mice²¹. These facts suggest a central role of Slack in the control of neuronal excitability, as both, too much as well as too little Slack activity increases seizure susceptibility.

In this study, using an *in vivo* epilepsy model, neuronal culture systems, live-cell imaging of Ca^{2+} and K^+ , and electrophysiology, we identify a neuroprotective role of Slack channels during acute epilepsy.

Methods

Animals. All experimental procedures were conducted in accordance with animal protection law in Germany and approved by the Ethics Committee for Animal Research (Regierungspräsidium Tübingen). Animals were maintained on a 12/12 h light/dark cycle (light on 6 a.m. to 6 p.m.) with access to food and water ad libitum. Slack-deficient mice (B6.129-Kcnt1^{tm1Ruth}/RoLu) were generated by targeted ablation of the Slack encoding gene *Kcnt1* in murine embryonic stem cells using a Cre/loxP-system³³. Founders were backcrossed to C57BL/6 N background for at least nine generations. Genotypes were determined by PCR after DNA extraction by KAPA2G Fast HotStart Genotyping Mix (KK5621, KAPA Biosystems, Sigma Aldrich Chemie GmbH, Taufkirchen, Germany). Primer sequences are listed in Supplementary Table 1. KA-based epilepsy model was performed with either 4 weeks-old (juvenile) or 12 weeks-old (adult) male litter-matched offspring from heterozygous (Slack^{+/−}) parental (P₂) animals. Subsequently, homozygous Slack^{+/+} or Slack^{−/−} animals (P₁) not used in epilepsy experiments were mated to generate age-matched homozygous Slack^{+/+} or Slack^{−/−} pups for *in vitro* experiments i.e., hippocampal brain slice cultures or dissociated cell cultures. This two-stage breeding strategy avoids the need to genotype P0 to P1 pups used for culturing, as would be required when using heterozygous breeders. At the same time, genetic drift between individual homozygous lines is prevented.

Kainic acid model for acute epilepsy. Susceptibility and seizure severity in Slack^{+/+} and Slack^{−/−} mice were assessed by using the KA-based model of acute epilepsy. KA (ab120100, Abcam, Berlin, Germany) dissolved in sterile saline was intraperitoneally applied to randomly selected litter-matched juvenile (20 mg/kg) or adult (30 mg/kg) male Slack^{+/+} and Slack^{−/−}. Injected animals were transferred to a vivarium for optimal observation and video recording for 90 min. Seizure severity was measured as seizure score (SSc) on an adopted Racine Scale as highest score reached in a 5 min interval. Score criteria ranged from SSc 0—no response, to SSc 1—immobile and rigid, SSc 2—myoclonic jerks and head nodding, SSc 3—forelimb clonus and Straub-tail, SSc 4—rearing with forelimb clonus, SSc 5—rearing, falling and jumping, SSc 6—tonic-clonic seizures with status epilepticus (SE) and SSc 7—seizures leading to death. Following observation, animals recovered in their home cage for 24 h before euthanasia. Hippocampi were dissected from removed brains in ice-cold DPBS (14190-094, Thermo Fisher Scientific, Waltham, US) and snap-frozen in liquid nitrogen for subsequent mRNA isolation.

Organotypic hippocampal slice cultures. Hippocampal slice cultures (HSC) were obtained from postnatal day 5 (P5) pups of both sexes. Pups were decapitated and brains removed. Hippocampi were dissected in ice-cold dissecting medium, composed of HBSS (14025, Thermo Fisher Scientific), 20 mM HEPES, and 20 mM D-glucose (both obtained from Carl Roth GmbH + Co. KG, Karlsruhe, Germany) using an iris spatula (10093-13, Fine Science Tools, Heidelberg, Germany) following by midsagittal division of hemispheres. 400 μm transversal slices were cut on a McIlwain tissue chopper (Quantum Design GmbH, Darmstadt, Germany). Complete and undamaged hippocampal sections were selected for subsequent culturing in 6-well plates. 5 slices were placed in each well onto 0.4 μm membrane inserts (PICM03050, Merck Millipore, Darmstadt, Germany) with 1 ml of culturing medium (MEM, 32360034, Thermo Fisher Scientific), supplemented with 20% horse serum (26050088, Thermo Fisher Scientific), 1 mM GlutaMAX (35050061, Thermo Fisher Scientific), 0.000125% ascorbic acid (A92902, Sigma), 0.001 mg/ml insulin (I2643, Sigma), 1 mM CaCl_2 , 2 mM MgSO_4 , 20 mM D-glucose (all Carl Roth GmbH + Co. KG), and 100 U/ml penicillin/streptomycin (15140122, Thermo Fisher Scientific). Medium was changed after 3 h and subsequently every 3 days for up to 14 days *in vitro* (div). Cultures were maintained in a humidified HeraCell150 Incubator (Thermo Fisher Scientific) at 37 °C with 5% CO_2 . Slices underwent flattening during the first 10 days and appeared transparent with clearly visible hippocampal compartments until 14 div.

Dissociated hippocampal neuronal cultures. Primary hippocampal neurons (PHN) were prepared and cultured from P0 Slack^{+/+} and Slack^{−/−} pups of both sexes according to the established protocol described below²². Pups were decapitated and brains transferred to ice-cold dissecting medium (HBSS, 10 mM HEPES, 1 mM sodium pyruvate (Thermo Fisher Scientific, 0.1% D-glucose)). Hippocampi were isolated as described for HSC and freed from meninges. After washing in dissecting medium, hippocampi were incubated with trypsin (0.25%, 15090, Thermo Fisher Scientific) at 37 °C for 20 min before 0.1% Desoxyribonuclease I (DN25, Sigma Aldrich Chemie GmbH) was added for another 5 min at room temperature. Next, hippocampi were washed with dissecting and plating medium (BME with EBSS, 41010-026, Thermo Fisher Scientific), 10% fetal bovine serum (16140071, Thermo Fisher Scientific; 0.45% D-glucose, 1 mM sodium pyruvate and 2 mM GlutaMAX, 100 U/ml P/S).

Hippocampi were dissociated by gentle trituration in plating medium with fire-polished Pasteur pipets and subsequently seeded onto poly-L-Lysine coated coverslips (0.5 mg/ml, P2636, Sigma Aldrich Chemie GmbH). 110,000 cells in plating medium were either plated on 32 mm diameter coverslips restricted by silicon culture inserts (80466, ibidi GmbH, Graefelfing, Germany) to reduce growth area, or on 12 mm coverslips. 2 h after seeding, medium was changed to maintenance medium (Neurobasal, 21103049, Thermo Fisher Scientific with B-27, 17504044, Thermo Fisher Scientific and 2 mM GlutaMAX) and kept in culture for 8 to 14 days by changing 30% of medium every 4 days.

Propidium iodide-based cell death assay. KA-induced cell death in HSC and PHN was assessed using propidium iodide (PI) staining. Basal viability of 14 div HSC was measured after 10 min incubation with 2 μ g/ml PI (P4864, Sigma Aldrich Chemie GmbH) using an RFP filter block in a Nikon Eclipse Ts2R microscope (Nikon Instruments Inc., Melville, US) Plan Fluor OFN25 \times 4 objective (Nikon Instruments Inc.) and a DMK 33Ux174 camera (oem cameras, Middletown, US). PI uptake was measured 24 h after the addition of 5 or 10 μ M KA to the medium. To provide a KA-independent positive control at the end of each experiment, culturing medium was replaced by 1 ml of 80% EtOH for 1 h at -20° C before new PI was re-applied for a final set of images. Relative PI uptake was quantified as described³⁴ by using Fiji³⁵. Three circular regions of interest (ROI, 80 \times 80 pixels) were placed on each CA1/2, CA3/4, and dentate gyrus. An additional tenth region was placed adjacent to the slice for background subtraction. Background subtracted integrated densities of each region were averaged for each hippocampal compartment. KA-induced PI uptake was calculated relative to the positive control for each slice following the subtraction of basal PI uptake.

For cell death detection of dissociated neurons, PHN were plated on ibidi 8 well chamber slides (80826, ibidi GmbH) and cultured for 8 to 14 div. For measurement, PI (2 μ g/ml) and KA (5 or 10 μ M) were added to each well. In a second set of experiments, PHN was treated for 24 h with 10 μ M KA and 50 or 100 μ M picrotoxin (PiTX). Slides were placed into a prewarmed stage top incubation system (10722, 11922-DL, 10918-DL, ibidi GmbH) maintaining 5% CO₂, 21% O₂, and 80% humidity at 37° C. For each well, time courses from 4 to 5 ROI were automatically imaged using a BioPrecision2 automated XY-table (Ludl Electronic Products Ltd., Hawthorne, US) on a Zeiss Axio Observer Z1 inverted microscope equipped with a Zeiss EC-Plan-Neofluar \times 20/0.5 objective (440340-9904, Carl Zeiss AG, Oberkochen, Germany) and a LedHUB LED light-engine equipped with 505–600 nm LED (Omicron Laserage Laserprodukte GmbH, Dudenhofen, Germany). Filter set (475/543/702 nm) was obtained from AHF Analysetechnik. PI emission was automatically detected every 30 min for 24 h with a PCO panda 4.2bi camera (Excelitas PCO GmbH, Kelheim, Germany) controlled by VisiView software (Visitron Systems GmbH, Puchheim, Germany). Fiji was used to count particles in each ROI over time after background subtraction and application of a constant threshold to calculate relative PI uptake to basal number of particles.

Immunofluorescence staining. Slack expression and maturity of dissociated hippocampal cultures were verified by staining against MAP2 at 8 and 14 div. First, cells were washed twice with warm HBSS and fixed for 10 min with warm fixation solution (DPBS, 14190-094, Thermo Fisher Scientific with, 4% Paraformaldehyde and 4% sucrose (Carl Roth GmbH + Co. KG)). Cells were washed twice and incubated for 2 h at room temperature with blocking solution (DPBS with 2% Glycerol, 0.3% Triton X-100, 50 mM NH₄Cl, 5% NGS Vector Labs S-1000, 2% BSA (0163.2, Carl Roth GmbH + Co. KG)). Subsequently, cells

were incubated with primary antibodies (1:300 monoclonal anti-KCNT1, SAB5200036, Sigma Aldrich Chemie GmbH, 1:1500 monoclonal MAP2, D5G1, Cell Signaling Technology, Leiden, Netherlands) in blocking buffer for 24 h at 4° C. Next, cells were washed in washing solution (DPBS with 0.01% Triton X-100) and incubated for 2 h at room temperature with secondary antibodies (Alexa555, A21127, Alexa488, A11034, Thermo Fisher Scientific) and Hoechst 33342 (1:1000) in blocking buffer. Cells were washed in washing solution, DPBS, and water. Cells were mounted with PermaFluor aqueous mounting medium (TA-030-FM, Thermo Fisher Scientific) and imaged the next day with a Zeiss Axiovert 200 M equipped with a color camera (AxioCam MRc Rev 3) and ZEN 3.4 software (Carl Zeiss AG).

Ca²⁺ imaging. 8 to 14 div PHN loaded with 2.5 μ M Fura-2AM (21021, Biomol GmbH, Hamburg, Germany) in maintenance medium for 40 min and were subsequently transferred to a PC30 perfusion chamber (NGFI GmbH, Graz, Austria) connected to a gravity-based perfusion system (NGFI GmbH) to obtain constant perfusion with prewarmed recording buffer (in mM: 138 NaCl, 5 KCl, 2 CaCl₂, 1 MgCl₂, 10 HEPES, 10 D-glucose). Intracellular Ca²⁺ concentration ([Ca²⁺]_i) was measured using a Zeiss Axiovert 200 equipped with a Zeiss Fluar 440255 \times 40/1.30 oil immersion objective (Carl Zeiss AG) and illuminated by a CoolLED pE-340^{fura} (CoolLED Ltd, Andover, US). The light was filtered by AHF Analysetechnik F39-380 and F39-343 nm BrightLine, passed the dichroic filter AT515LP, and the emission was finally filtered by CmF 525/15. Fura-2 was imaged at 1 Hz, with a binning of 4 using a PCO panda 4.2 camera (Excelitas PCO GmbH) and VisiView software (Visitron Systems GmbH) with background correction. After 2 min measurement of basal [Ca²⁺]_i, PHN was superfused for 2 min with recording buffer containing 1 to 100 μ M KA before washout for 3 min. Maximum change in fluorescence emission ratio between excitation at 340 nm and 340 nm was calculated. All cells from one recording were averaged and data was analyzed using GraphPad Prism 8 (GraphPad Software, Boston, US).

K⁺ imaging. After 8–14 div PHN were virally transduced with an adeno-associated virus-DJ/8 vector system encoding the cytosol targeted K⁺ sensitive, FRET-based biosensor NES lc-LysM GEPII 1.0³⁶ under control of a CAG promoter at a multiplicity of infection (MOI) of 100. PHN were imaged 72 h after transduction in a PC30 perfusion chamber (NGFI GmbH) under constant perfusion with prewarmed imaging buffer (in mM: 126.5 NaCl, 5 KCl, 2 CaCl₂, 2 MgCl₂, 10 HEPES, 30 D-glucose, 10 sodium pyruvate) by a gravity-based perfusion system (NGFI GmbH). Imaging was performed using a Zeiss Axio Observer Z1 inverted microscope equipped with a Zeiss EC Plan-NEOFLUAR \times 40/1.3 Oil 420460-9900 objective (Carl Zeiss AG) and connected to a LedHUB LED light-engine producing excitation light at a wavelength of 430 nm (Omicron Laserage Laserprodukte GmbH). The filter set was obtained from AHF Analysetechnik for 427/10 nm. Emission light of GEPII 1.0 was collected simultaneously at 475 and 530 nm using an Optosplit II optical image splitter (Cairn Research, Faversham, UK) equipped with a T505lpxr (AHF Analysetechnik) for CFP/YFP connected to a PCO panda 4.2bi camera (Excelitas PCO GmbH). Images were acquired at 1 Hz with a binning of 4 using VisiView software (Visitron Systems GmbH). Ratios were calculated after background correction by YFP to CFP division and the ratio was normalized for first 2 min of baseline recording to obtain maximal changes in YFP/CFP ratios during KA stimulations. All cells from one recording were averaged and further data analysis was performed using GraphPad Prism 8 (GraphPad Software).

Electrophysiology. Coverslips with 14 div PHN were transferred to a submerged-type recording chamber (Warner Instruments USA) constantly perfused with extracellular buffer (in mM: 140 NaCl, 2.5 KCl, 2 CaCl₂, 4 MgCl₂, 10 HEPES, 10 D-glucose, pH 7.4, 300 mOsm/kg). Cells were visualized by a Nikon Tc2R equipped with a Nikon S Plan Fluor $\times 40/0.6$ objective with EMBOSS contrast and a DFK 33Ux174 camera (Nikon Instruments Inc.). 3.5–4 M Ω micropipettes were pulled from borosilicate glass (BM150-10P, Science Products GmbH, Hofheim, Germany) using a P-1000 Micropipette Puller (Sutter Instruments, Novato, US) and polished by a MF-830 Micro Forge (Narishige International Ltd., London, UK) and filled with intracellular buffer (in mM: 136 K-gluconate, 0.6 MgCl₂, 17.8 HEPES, 1 EGTA, 4 Mg-ATP, 0.3 Na²-GTP, pH 7.4, 300 mOsm/kg). Whole-cell recordings were sampled at 5 kHz using an EPC10 amplifier (HEKA Elektronik GmbH, Lambrecht, Germany) and PatchMaster software. Whole-cell capacitance and series resistance were compensated. Cells with changes in access resistance exceeding 20% during recording were excluded from the analysis. Data was analyzed using FitMaster software. Cells were held at -60 mV and whole-cell current responses to 500 ms voltage steps between -60 to $+80$ mV in 20 mV increments were recorded before and after perfusion with 10 μ M tetrodotoxin (TTX, Carl Roth GmbH + Co. KG). Minimum current amplitude in a 15 ms window at the beginning and mean amplitude in the last 25 ms of the depolarizing pulse were used to measure transient inward currents and steady-state currents, respectively.

5 μ M KA were added to neurons held in current-clamp mode near -60 mV. Starting from the first KA-induced AP, the number of APs per 1 s bin was counted for 30 s as well as AP threshold (membrane potential at AP initiation) and amplitude (from threshold to peak). For current injections, cells were held near -60 mV in current-clamp mode and depolarized by 10 current injections in increments of 20 pA for 500 ms. AP number per depolarization as well as AP threshold (membrane potential at AP initiation), AP amplitude (from threshold to peak) and afterhyperpolarization (aHP) duration (time from HP peak to resting potential³⁷), and amplitude (aHP peak minus resting potential) were measured for the first AP. Maximal AP rise slope, maximal AP decay slope, and AP halfwidth were analyzed using threshold-based event-detection of Clampfit 10.7 (Molecular Devices LLC).

Quantitative RT-PCR. Hippocampi were isolated 24 h after KA-induced seizures, homogenized (Polytron PT 1200E), and extracted in 1 ml Peq-GOLD RNApure (VWR International GmbH, Darmstadt, Germany) according to manufacturer's instructions. mRNA was extracted from 20 pooled hippocampal brain slice cultures using the NucleoSpin kit (MACHEREY-NAGEL GmbH & Co. KG, Düren, Germany) according to manufacturer's instructions. Genomic DNA was digested using DNase I (04716728001, Sigma Aldrich Chemie GmbH,) at 54 °C for 30 min. 500 ng RNA was reversely transcribed by iScript cDNA Synthesis Kit (170-8896, Bio-Rad Laboratories GmbH, Feldkirchen, Germany). Real-time quantitative PCR (RT-PCR) was performed in triplicates with 7.5 ng/ μ l mRNA and 333 nmol/l of corresponding primers. Each run included water and reverse transcriptase (RT) negative controls (where RT was omitted during reverse transcription). Reactions were performed using SSoAdvanced Universal SYBR Green Supermix (1725274, Bio-Rad Laboratories GmbH) on a CFX Connect Real-Time PCR Detection System (Bio-Rad Laboratories GmbH) by incubating at 92 °C for 2 min, followed by 40 cycles of 5 s at 95 °C and 30 s at 58 °C. Expression of targeted genes was calculated by the 2 $^{-\Delta\Delta Ct}$ method relative to hypoxanthine-guanine phosphoribosyl transferase (HPRT). Primer sequences

were designed by Primer3 and PrimerBLAST software and are listed in Supplementary Table 1.

Statistics and reproducibility. Data were analyzed using GraphPad Prism version 8 (GraphPad Software). First, D'Agostino & Pearson test for normality distribution was performed, followed by the appropriate outlier test. Genotype-dependent effects were analyzed by unpaired t-test including Welch's correction in case of different variance, Mann-Whitney test in case of non-parametric data, and two-way ANOVA in case of time course-related data. Juvenile mice also died following KA-induced seizures, so mRNA transcript levels were analyzed between surviving and dead animals. Since no genotype-specific effects were found, all Slack^{-/-} samples were pooled. Fraction of animals that reach different SSc upon KA injection was reported as part of the whole and in percent (Fig. 1c, f). Differences were statistically assessed by χ^2 test, although its meaningfulness is somewhat limited for small numbers³⁸. In the case of Fura-2 measurements with increasing KA concentrations, a non-linear, sigmoidal curve fit was performed to determine the logEC₅₀ and goodness of curve fit. Sample size (*N* value) is defined as number of animals for KA-based epilepsy testing. For quantification of KA-induced PI uptake in HSC *n* was defined as mean of three regions placed in each, CA1, CA3, and DG of 5 slices cultured together in one well. Slices of 3 to 6 preparations were analyzed. For quantification of KA-induced PI uptake in PHN, sample size *n* was defined as ROI with four to five ROI per well and recording. Recordings were performed from three preparations. For Fura-2-based Ca²⁺ measurements and FRET-based K⁺ measurements cells of each measurement were averaged to one experimental sample *n*. Data are acquired from 8 to 10 preparation and 12 to 13 wells. For patch-clamp experiments, each cell was defined as one sample *n* and data analysis based on 6 to 7 preparations for voltage-clamp data and 8 to 9 preparations for current-clamp data. All data are represented as mean \pm SEM. In figures, significance is indicated by asterisks (* $p < 0.05$, ** $p < 0.01$, *** $p < 0.001$). n.s. denotes non-significant results ($p > 0.05$). Statistics are listed together with raw data in Supplementary Data 1.

Reporting summary. Further information on research design is available in the Nature Portfolio Reporting Summary linked to this article.

Results

Slack^{-/-} mice are more susceptible to kainic acid-induced acute epilepsy. First, we aimed to elucidate Slack's role in acute seizures by applying the widely studied KA-based model. Seizures were provoked by injection of 30 mg/kg KA in 12 weeks-old male mice. Animals were observed over 90 min and scored in 5 min intervals using an adopted Racine Scale. Within 20 min, KA injection provoked convulsive behavior with seizure score (SSc) 3 and higher in both genotypes. Overall SSc was significantly increased in Slack^{-/-} compared to Slack^{+/+} (Fig. 1a). Time to reach convulsive seizures (CS) with a SSc of ≥ 3 was similar for both genotypes (Fig. 1b). Additionally, the fractions of Slack^{-/-} developing SE (Slack^{+/+}: 1 of 7; Slack^{-/-}: 4 of 7) was increased but this difference was not significant ($p = 0.09$) while there was a clear tendency ($p = 0.05$) for a higher probability of Slack^{-/-} (Slack^{+/+}: 0 of 7; Slack^{-/-}: 3 of 7) to die from seizures (Fig. 1c). Since Slack-related epilepsy syndromes in human carriers of pathogenic KCNT1 variants are characterized by early onset, we also injected 4 weeks-old juvenile male mice with 20 mg/kg KA. Juvenile mice of both genotypes responded with severe convulsions and reached SSc ≥ 4 within 20 min after KA application (Fig. 1d), with a similar time of onset of CS (Fig. 1e). While the fraction of animals reaching SE

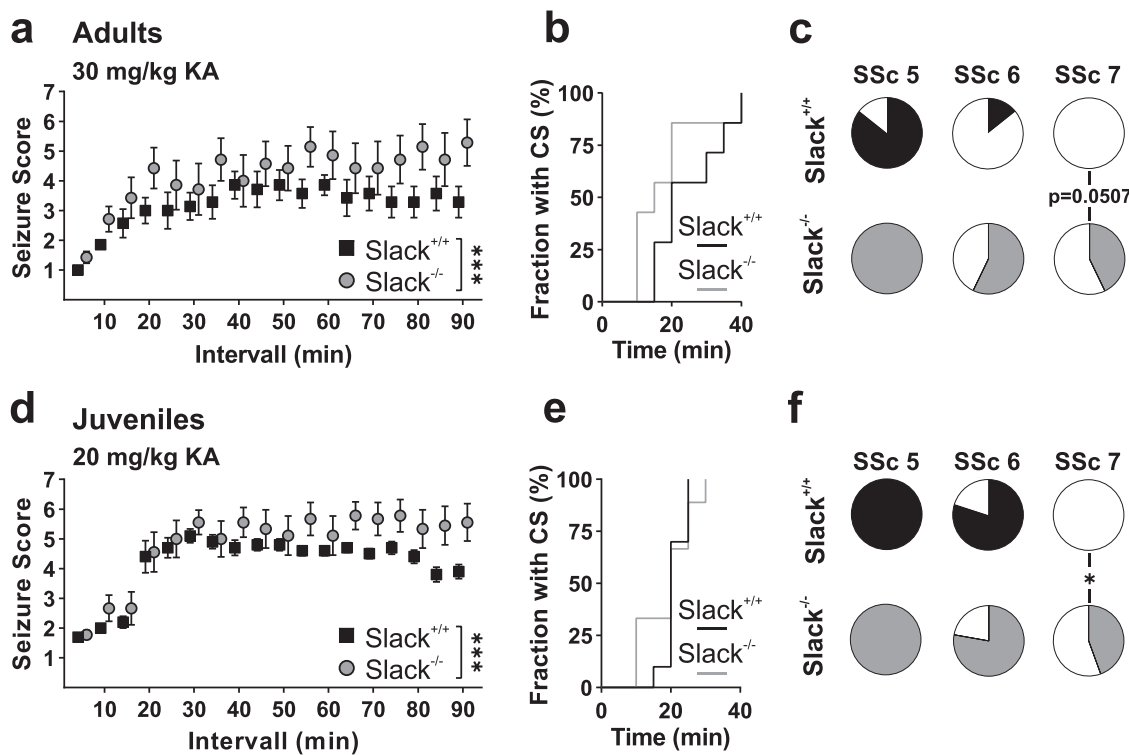


Fig. 1 Increased severity and lethality of kainic acid-induced seizures in *Slack*^{-/-}. a 12 weeks-old adult male wildtype (*Slack*^{+/+}) and knockout (*Slack*^{-/-}) mice were tested for seizure susceptibility and severity by injection of 30 mg/kg KA i.p. Seizures were scored using an adopted Racine Scale (from Seizure Score 0 (SSc 0), no seizures, to SSc 6, SE, and SSc 7, death after SE). Compared to *Slack*^{+/+} ($N = 7$), *Slack*^{-/-} ($N = 7$) animals display significantly ($p < 0.001$; two-way ANOVA $F_{1,216} = 24.32$) increased seizure severity over time, with b a similar onset of convulsive seizures (CS, SSc ≥ 3) but c more frequent occurrence of tonic-clonic seizure (SSc 6) and almost significantly more frequent death (SSc 7) (χ^2 , $p = 0.0507$) following SE (black and gray sectors in c represent the affected, white sectors the unaffected fraction of animals by genotype for each respective SSc). Fractions of animals with SSc ≤ 5 were similar for both genotypes. d 4-week-old juvenile mice were tested for seizure susceptibility and severity by i.p. injection of 20 mg/kg KA and scoring. Compared to *Slack*^{+/+} ($N = 10$), *Slack*^{-/-} ($N = 9$) animals display significantly ($p < 0.001$; two-way ANOVA $F_{1,144} = 30.63$) increased seizure severity over time with e similar onset of CS but f significantly more frequent death (SSc 7) (χ^2 , $p = 0.017$) following SE (black and gray sectors in f represent the affected, white sectors the unaffected fraction of animals by genotype for each respective SSc). Response to SSc ≤ 5 was similar for both genotypes. Data represented as mean \pm SEM. For detailed statistics also consult Supplementary Data 1.

(*Slack*^{+/+}: 8 of 10; *Slack*^{-/-}: 7 of 9) was not different, *Slack*^{-/-} showed significantly increased seizure-induced lethality (*Slack*^{+/+}: 0 of 10; *Slack*^{-/-}: 4 of 9) compared to *Slack*^{+/+} (Fig. 1f). Interestingly, by analyzing mRNA expression levels of related channel subunits 24 h following KA-induced seizures, no prominent alterations were found in either genotype (Supplementary Fig. 1a–f), despite a significantly decreased level of BDNF in *Slack*^{-/-} (Supplementary Fig. 1f). These results demonstrate that KA-induced seizures are more severe in adult and juvenile *Slack*^{-/-}, which suggests that *Slack* channels acutely limit epileptic neuronal activity in vivo.

Kainic acid amplifies cell death in *Slack*^{-/-}. The limbic system, especially the hippocampal formation is prone to be focused for ictal events and epileptic seizures, leading to hippocampal sclerosis and temporal lobe epilepsies³⁹. Furthermore, *Slack* channels²¹ and KA receptors (GluK)^{40,41} are also highly expressed in the hippocampus and KA injection is known to produce neuronal cell death in different hippocampal layers. We therefore assessed sensitivity to KA-induced cell death of hippocampal neurons in vitro by quantifying propidium iodide (PI) uptake. First, we used HSC, a model in which physiological intrahippocampal synaptic connections remain preserved⁴². 24 h exposure of isolated HSCs to 5 or 10 μ M KA significantly increased cell death in cultures from *Slack*^{-/-} compared to *Slack*^{+/+}

(Fig. 2a, b). PI uptake seemed to be highest in CA3 (see Fig. 2a middle, Supplementary Fig. 2), which is the hippocampal area with the highest GluK expression as well as the one that is most susceptible to degeneration due to hippocampal sclerosis and temporal lobe epilepsy³⁹. Next, we tested if the effects observed in cultures from *Slack*^{-/-} might be due to expressional changes of closely related K⁺ channels. Transcript levels of the related and highly homologous Na⁺-, or Ca²⁺-activated K⁺ channels Slick and BK, however, were unchanged between both genotypes in mature HSC, contradicting compensatory regulation of these two K⁺ channels under pathophysiological conditions (Fig. 2c).

Subsequently, we analyzed KA-induced cell death in 8 to 10 div cultures from dissociated *Slack*^{+/+} and *Slack*^{-/-} hippocampal neurons to observe cell-autonomous effects independent from intrahippocampal synaptic connections. MAP2-expressing 8–10 div hippocampal *Slack*^{+/+} neurons show robust *Slack* immunoreactivity which is absent in *Slack*^{-/-} (Fig. 3a). Subsequently, neuronal cultures were again exposed to either 5 or 10 μ M KA over 24 h. In accordance with our findings in HSC, cell death in *Slack*^{-/-} neurons exposed to 10 μ M KA was significantly increased in comparison to *Slack*^{+/+} (Fig. 3b, c). To assess whether this observed cell death is due to increased neural activity, we co-treated PHN with 50 or 100 μ M of the GABA_A inhibitor picrotoxin (PiTX) to increase neuronal excitability. As expected, PiTX dose-dependently led to significantly amplified KA-induced cell death in both genotypes, indicating excessive neuronal activity to drive neuronal

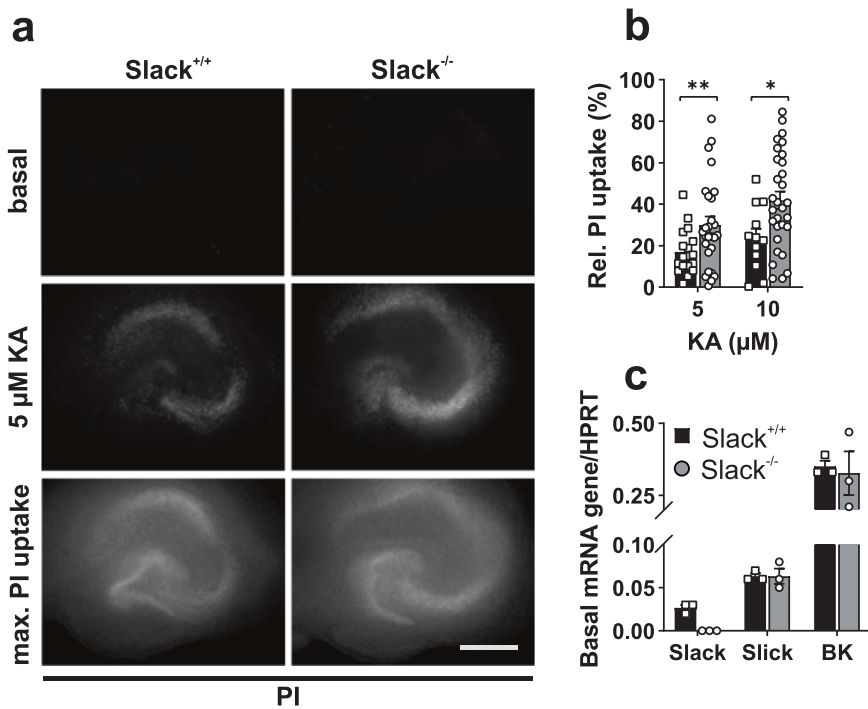


Fig. 2 Increased KA-induced cell death in Slack^{-/-} organotypic hippocampal slice cultures. **a** Representative images of 14 div slice cultures from Slack^{+/+} and Slack^{-/-} before (basal) treatment, after 24 h treatment with 5 μM KA, and after application of 80% ethanol (max. PI uptake). Scale bar: 500 μm. **b** Compared to Slack^{+/+}, Slack^{-/-} slice cultures show significantly increased PI uptake (normalized to maximum) in response to 24 h treatment with 5 μM (Slack^{+/+} $n = 18$ ROI out of four preparations, Slack^{-/-} $n = 27$ ROI out of six preparations, unpaired t test with Welch's correction $p = 0.009$) and 10 μM KA (Slack^{+/+} $n = 12$, Slack^{-/-} $n = 24$, unpaired t test $p = 0.016$). **c** mRNA from 14 div Slack^{+/+} and Slack^{-/-} hippocampal slice cultures, isolated for quantitative RT-PCR analysis. No Slack mRNA is detected in Slack^{-/-}. Slick and BK mRNA expression levels are similar in Slack^{+/+} and Slack^{-/-}. Data in **b**, **c** represented as mean ± SEM with $p < 0.05$ and $p < 0.01$. For detailed statistics also consult Supplementary Data 1.

demise (Fig. 3d). Under conditions of simultaneous treatment with KA and PiTX, however, cell death was not significantly different between genotypes within the individual conditions, but on a group level (see Supplementary Data 1). Taken together, increased cell death in Slack^{-/-} HSC and dissociated hippocampal neuron cultures provide *in vitro* confirmation of Slack's neuroprotective role, which was initially revealed by *in vivo* experiments.

Kainic acid-induced Ca^{2+} influx and K^+ efflux is increased in Slack^{-/-} hippocampal neurons. In order to elucidate the molecular processes underlying the increased vulnerability of Slack^{-/-} animals to KA-induced seizures and increased demise of Slack^{-/-} cells after KA stimulation, we performed single-neuron live recordings of $[\text{Ca}^{2+}]_i$ and $[\text{K}^+]_i$ concentrations in the presence or absence of KA. KA-induced $[\text{Ca}^{2+}]_i$ increases were observed after perfusion of 8 to 10 div hippocampal neurons loaded with Fura-2AM (Fig. 4a). Robust abrogation of the Ca^{2+} signal by extracellular EGTA verified the extracellular space as source for the KA-stimulated $[\text{Ca}^{2+}]_i$ increase (Fig. 4b). Subsequently, PHN were perfused with KA concentrations from 1 to 100 μM, and maximal delta ratios observed in Fura-2 emission ratios fitted a sigmoidal concentration-response curve (Fig. 4c). EC₅₀ values did not differ between Slack^{+/+} (EC₅₀ = 13.56 μM) and Slack^{-/-} (EC₅₀ = 13.78 μM) indicating similar GluK densities in neurons from both genotypes, while $[\text{Ca}^{2+}]_i$ of Slack^{-/-} appeared to be increased at 1 μM KA ($p = 0.002$).

To investigate the role of Slack-mediated K^+ currents during KA stimulation, we monitored $[\text{K}^+]_i$ in 8–10 div hippocampal neurons transduced with the genetically encoded potassium sensor NES lc-LysM GEPPII 1.0 (Fig. 4d). Interestingly, stimulation with 1, 3 and 5 μM KA provoked significantly stronger reduction of $[\text{K}^+]_i$ in Slack^{-/-} than in Slack^{+/+} (Fig. 4e, f). Taken together, live-cell

imaging data suggest that KA stimulation leads to increased Ca^{2+} influx as well as increased K^+ efflux in Slack^{-/-} neurons. Even though the latter result was somewhat counterintuitive.

Slack^{+/+} hippocampal neurons display Slack-specific TTX-sensitive outward currents and limited excitability. We next examined whether the changes in Ca^{2+} and K^+ homeostasis observed in Slack^{-/-} neurons translate into altered ion conductances and neuronal excitability. To this end, we first performed voltage-clamp recordings of 14 div PHN to observe whole-cell currents in response to depolarizing voltage steps. Tetrodotoxin (TTX), a blocker of voltage-gated Na^+ channels, was applied to isolate currents conducted by Na^+ channels as well as Na^+ -dependent K^+ channels (Fig. 5a, b). Depolarization-induced transient inward current densities were significantly higher in Slack^{-/-} than Slack^{+/+} neurons (Fig. 5b, c). Additionally, we observed significantly altered TTX-sensitive steady-state current densities between both genotypes (Fig. 5d). This difference is due to reduced outward current densities at depolarized membrane potentials, likely representing the lack of Na^+ -activated K^+ currents in Slack^{-/-}. Additionally, we also noticed a pronounced inward deflection of Slack^{-/-} steady-state currents between -40 and $+20$ mV (Fig. 5d with red line and e). This might be due to the increased expression of an inward-directed current component in Slack^{-/-}, likely persistent Na^+ currents (I_{NaP}), which were previously observed in *Drosophila* neurons lacking the Slack analog Slo2⁴³ as well as in mammalian neurons^{11,17}. These findings indicate that Slack^{-/-} neurons lack TTX-sensitive K^+ currents and also display changes in inwardly directed current components.

To examine, if the observed changes in TTX-sensitive currents influence neuronal activity, we performed current-clamp recordings

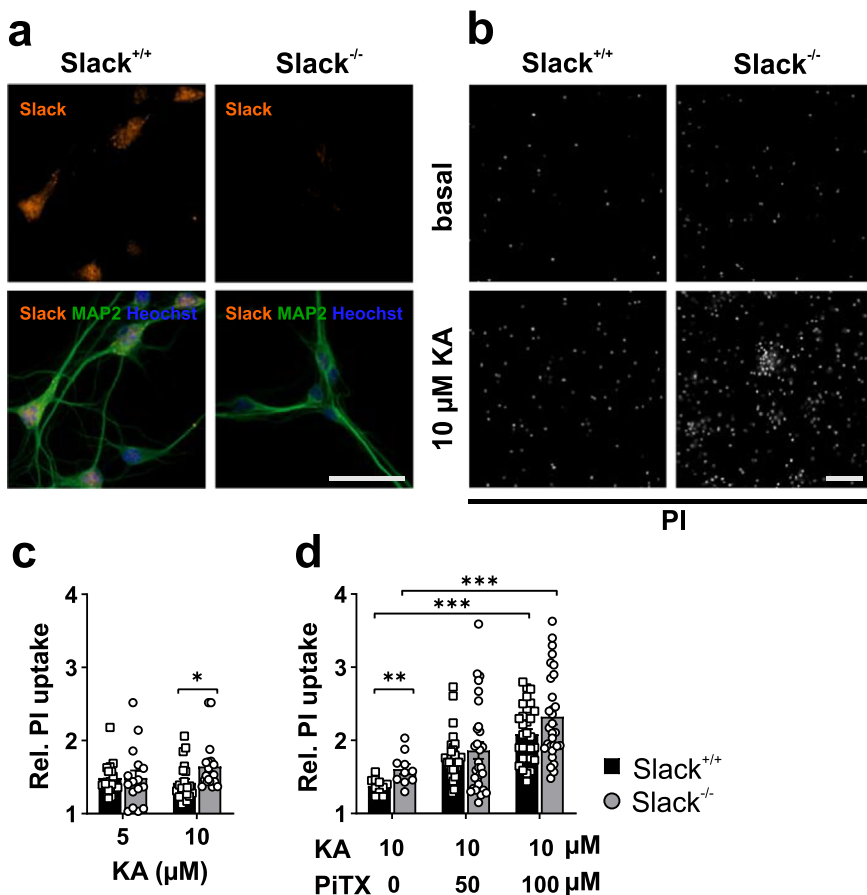


Fig. 3 Increased KA-induced cell death in Slack^{-/-} dissociated hippocampal neurons. **a** Representative fluorescence images of 8 div hippocampal Slack^{+/+} and Slack^{-/-} neurons stained with specific antibodies against Slack (red) and MAP2 (green). Nuclei were visualized with Hoechst 33342 (blue). Slack immunoreactivity is not detected in Slack^{-/-}. Scale bar: 40 μ m. **b** Representative images of PI uptake in 8 div hippocampal neurons before (basal, top) and after 24 h exposure to 10 μ M KA (bottom). Scale bar: 500 μ m. **c** Cell death is significantly increased (Mann-Whitney test, $p = 0.0016$) in Slack^{-/-} ($n = 22$ ROI out of three preparations) compared to Slack^{+/+} ($n = 20$ ROI out of three preparations) as measured by PI uptake (normalized to basal) after 24 h exposure to 10 μ M KA. **d** PI uptake in response to 10 μ M KA is significantly amplified by 24 h co-treatment with 100 μ M PiTX (Slack^{+/+} $n = 30$ ROI out of three preparations, Slack^{-/-} $n = 30$ ROI out of three preparations, Sidak's multiple comparison $p = 0.0008$ for Slack^{+/+}, $p = 0.0007$ for Slack^{-/-}). Slack^{-/-} PHN are overall more affected than Slack^{+/+} (two-way-ANOVA, $F_{1,134} = 4.270$, $p = 0.040$). Data in **c** represented as mean \pm SEM with $p < 0.05$, $p < 0.01$ and $p < 0.001$. For detailed statistics also consult Supplementary Data 1.

of 14 div PHN during bath application of KA. AP frequencies in 1 s bins recorded from the first AP after application of 5 μ M KA were significantly increased in Slack^{-/-} compared to Slack^{+/+} (Fig. 6a, b). This effect was accompanied by AP generation at tendentially more negative membrane potentials in Slack^{-/-} (Fig. 6c), while AP amplitude remained unchanged between genotypes (Fig. 6d). Injection of depolarizing currents also provoked significantly higher AP frequencies for a given current amplitude in Slack^{-/-} than Slack^{+/+} (Fig. 6e, f). This increased excitability cannot be explained by an altered resting membrane potential (Fig. 6g). It might, however, be due to initiation of AP at significantly more negative membrane potentials in Slack-deficient neurons (Fig. 6h). Although peak amplitudes of the elicited AP or aHP were not different between genotypes (Fig. 6i and Supplementary Data 1), AP rise slope was significantly steeper in Slack^{-/-} neurons (Fig. 6j, k) while AP halfwidth was similar between genotypes (Fig. 6l). These changes in AP kinetics are congruent with the observed amplification of TTX-sensitive inward currents in Slack^{-/-} (Fig. 5). Additionally, Slack^{-/-} neurons showed a significantly shorter aHP duration resulting in earlier return to resting potential compared to Slack^{+/+}, which implies that Slack K⁺ channels limit neuronal firing patterns by prolonging aHP duration (Fig. 6m, n).

In summary, Slack deficiency alters densities of inwardly and outwardly directed TTX-sensitive conductances, the threshold potential for AP initiation, and shortens aHP duration to accelerate KA- and depolarization-induced AP firing frequencies.

Discussion

Here we demonstrate that adult and juvenile Slack^{-/-} mice suffer from increased severity of KA-induced seizures (Fig. 1). This finding is consistent with previously documented epileptogenic LOF mutation in human Slack channels^{31,32}. Furthermore, increased susceptibility to glutamatergic excitotoxicity of Slack^{-/-} was also shown earlier²¹ as well as increased seizure susceptibility in *Drosophila*⁴³ and mice⁴⁴. The effects observed here are most likely due to the lack of Slack expression and not due to compensation by the related K⁺ channels Slick and BK or ionotropic glutamate receptors, as the respective transcript levels in both genotypes are similar 24 h after seizures (Supplementary Fig. 1). Interestingly, transcript levels of the neurotrophic factor BDNF were lower at that time point (Supplementary Fig. 1f), indicating again that Slack^{-/-} fail to upregulate neurotrophic signaling after detrimental excitatory events, as previously observed after glutamate-induced excitotoxicity²¹. Interestingly,

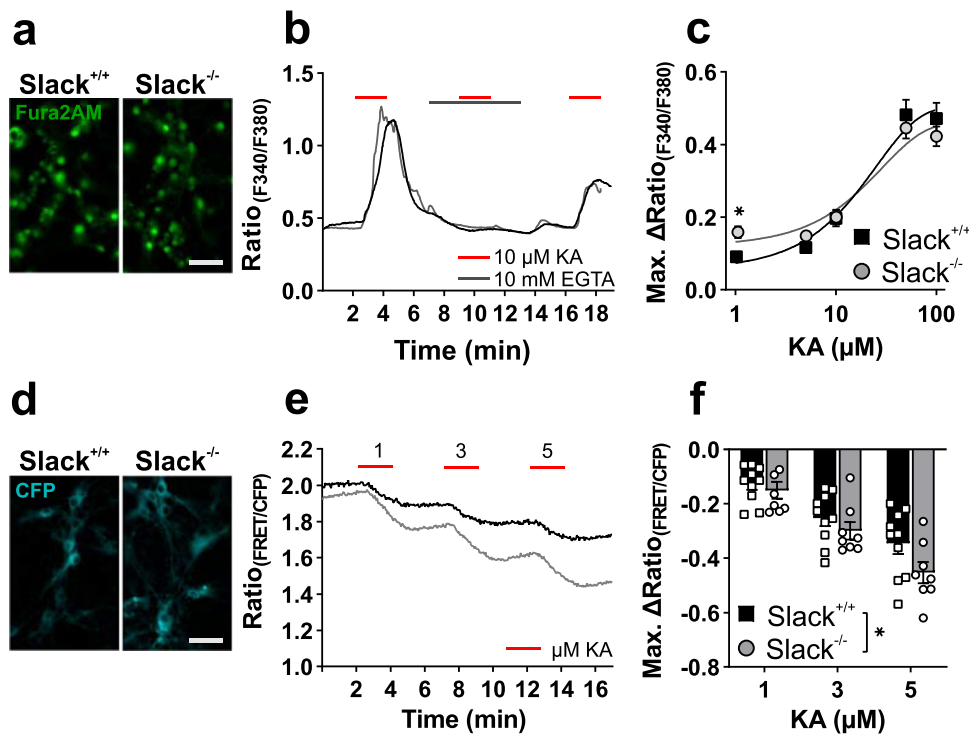


Fig. 4 Increased KA-induced Ca^{2+} influx and K^+ efflux in $\text{Slack}^{-/-}$ hippocampal neurons. **a** Representative images of Fura-2-loaded 8 div hippocampal neurons illuminated at 380 nm. Scale bar: 50 μm . **b** Representative time course of Fura-2 recordings in hippocampal neurons treated with 10 μM KA (red bar) alone or in presence of 10 mM EGTA (black bar). **c** Maximum change in ratio between fluorescence emission upon excitation at 340 nm and 380 nm in response to increasing KA concentrations. Concentration-response curves did not reveal differences between genotypes ($\text{Slack}^{+/+}$ $n=12-32$, $\text{EC}_{50}=13.56$, 95% IC = 9.14 to 20.11, $R^2=0.75$; $\text{Slack}^{-/-}$ $n=13-27$, $\text{EC}_{50}=13.78$, 95% IC = 8.92 to 21.29, $R^2=0.72$). Scale bar: 50 μm . At a low concentration of 1 μM KA, $\text{Slack}^{-/-}$ ($n=32$) responded with significantly increased Ca^{2+} influx compared to $\text{Slack}^{+/+}$ (Sidak's multiple comparison $p=0.013$, $n=27$). **d** Representative 8 div hippocampal neurons virally transduced with the FRET-based K^+ -sensitive sensor (GEPII). Scale bar: 50 μm . **e** Representative time course of $[\text{K}^+]$ recording with NES Ic-LysM GEPII 1.0 based FRET/CFP ratio in hippocampal neurons treated with indicated KA concentrations. **f** $[\text{K}^+]$ was significantly (two-way ANOVA, $F_{1,48}=4.8$, $p=0.031$) reduced in $\text{Slack}^{-/-}$ ($n=8$ wells out of five preparations) compared to $\text{Slack}^{+/+}$ ($n=10$ wells out of six preparations) neurons following treatment with 1, 3, and 5 μM KA. Data of **c**, **f** represented as mean \pm SEM with $p < 0.05$. For detailed statistics also consult Supplementary Data 1.

elevated seizure susceptibility of $\text{Slack}^{-/-}$ mice was previously demonstrated in an electroconvulsive model⁴⁴. In that study, however, $\text{Slack}^{-/-}$ mice showed increased post-ictal survival rates despite their increased sensitivity. This discrepancy might be due to different means of seizure induction. In contrast to KA injection, electric stimulation could preferentially activate cortical areas, leading to different excitatory and inhibitory excitation patterns. This fact, however, also indicates that Slack function may differentially affect the imbalanced neuronal activities in epileptogenesis depending on the involved cell types and brain areas as well as triggering non-genetic factors. Increased seizure severity in $\text{Slack}^{-/-}$ is in line with an earlier hypothesis of Slack's role as seizure terminator which was proposed shortly after the channel's identification⁴⁵. A great body of recent research, however, seems to contradict this notion, as GOF Slack variants appear to promote epilepsy development and severity in humans and mice^{25,44,46,47}. Traditionally, K^+ channels are seen as counter-epileptic agents^{48,49}, but three possible pathomechanisms were discussed for how Slack overactivity causes seizures²⁹. First, Slack channels increase AP frequencies by shortening voltage-gated Na^+ channel (Na_V) inactivation. Second, developmental alterations in synaptic connectivity led to the generation of hyperactive networks. Third, reduced excitability of inhibitory neurons disinhibits excitatory networks. In support of the latter theory, altered inhibitory signaling in vivo and in vitro was demonstrated in three different knock-in (KI) mouse models of Slack GOF variants^{44,46,47}. To reconcile this apparent

epileptogenicity of Slack with our finding of increased seizure severity in $\text{Slack}^{-/-}$, we must assume that too much as well as too little Slack activity possibly leads to detrimental neuronal activity in dependence on the involved brain regions. This raised the question of how the reduction or loss of Slack activity increases seizure incidence and severity.

Slack-mediated protection during KA-induced seizures was further explored by determining cell death after KA exposure in hippocampal brain slice cultures and primary dissociated hippocampal neurons. In agreement with our in vivo observations, both types of $\text{Slack}^{-/-}$ hippocampal cell preparations were more susceptible to KA-induced damage than controls (Figs. 2 and 3). In slice cultures, cell death was predominant in CA3 (Supplementary Fig. 2), the hippocampal region with the highest expression of Slack^{1,14} and GluK⁴⁰. Co-treatment of primary dissociated hippocampal neurons with PiTX exacerbated KA-induced cell death linking excessive neuronal activation by disinhibition to cell death (Fig. 3d). Overall, these experiments verified dissociated hippocampal neurons as a suitable model recapitulating important parts of the cellular events taking place during KA-induced seizures, which reportedly result in massive neuronal death⁴⁰. Next, $[\text{Ca}^{2+}]_i$ was measured in response to increasing KA concentrations to assess the cell biological events leading to cell death and PI uptake in this system. Indeed, Slack limits Ca^{2+} influx at lower but not at high KA concentrations (Fig. 4c). This suggests a reduced threshold for Ca^{2+} entry into $\text{Slack}^{-/-}$ neurons in agreement with the notion of K^+ channels as

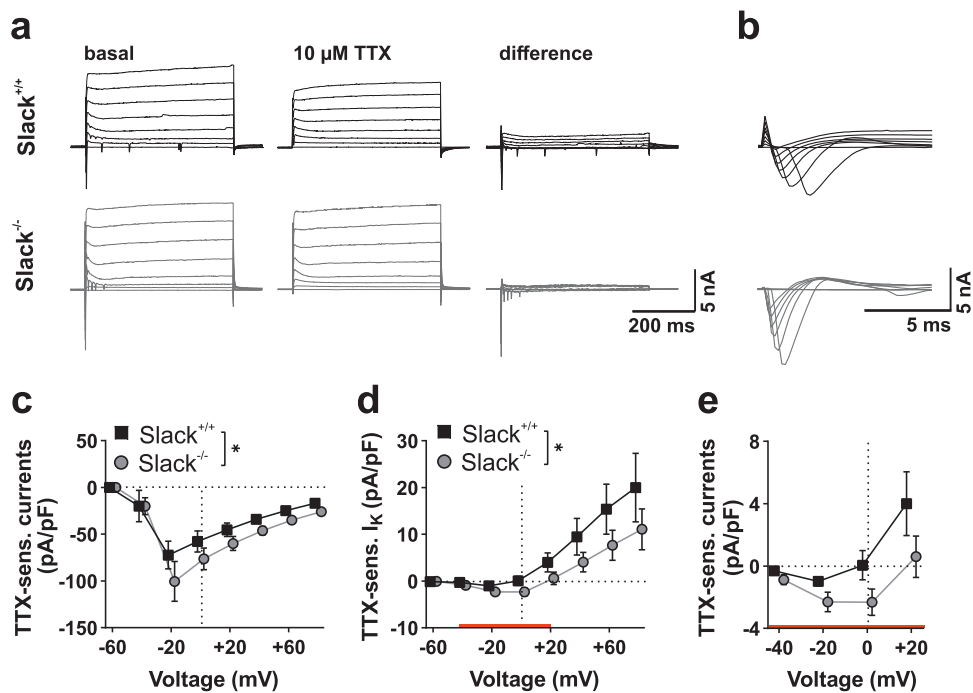


Fig. 5 Increased Na^+ currents in $\text{Slack}^{-/-}$ hippocampal neurons. **a-e** Voltage-clamp recordings of whole-cell currents from 14 div hippocampal neurons. **a** Representative recordings from $\text{Slack}^{+/+}$ and $\text{Slack}^{-/-}$ neurons responding to depolarizing voltage steps (from -60 to $+80$ mV in 20 mV increments) before (left), after perfusion with TTX (middle) and following digital subtraction (right). **b** (Magnification from **a**) Depolarization-induced, TTX-sensitive transient inward currents. **c** Compared to $\text{Slack}^{+/+}$ ($n=20$ from six preparations), TTX-sensitive inward current amplitudes in $\text{Slack}^{-/-}$ ($n=17$ from 7 preparations) neurons were significantly ($p < 0.0168$) increased (two-way ANOVA, $F_{1,280} = 5.791$). **d** TTX-sensitive steady-state outward currents were significantly (two-way ANOVA, $F_{1,312} = 5.122$, $p = 0.0243$) higher in $\text{Slack}^{+/+}$ ($n=24$) compared to $\text{Slack}^{-/-}$ ($n=17$). **e** (Magnification of red section from **d**) TTX-sensitive steady-state currents at voltage steps from -40 to $+20$ mV indicated an enlarged inward-directed current component in $\text{Slack}^{-/-}$ probably representing I_{NaP} . Data represented as mean \pm SEM with $p < 0.05$. For detailed statistics also consult Supplementary Data 1.

inhibitory components, while maximal activation of Ca^{2+} influx remains unaffected. Surprisingly, reduction of $[\text{K}^+]_{\text{i}}$ in response to 1, 3, and $5 \mu\text{M}$ KA was much stronger in $\text{Slack}^{-/-}$ (Fig. 4e, f). This finding indicates that exposing $\text{Slack}^{-/-}$ neurons to KA (see below) activates an additional K^+ conductance which, in turn, reduces $[\text{Ca}^{2+}]_{\text{i}}$ elevations (Fig. 4c). This data contrasts previous findings of decreased K^+ efflux from $\text{Slack}^{-/-}$ cerebellar granule cells after treatment with $300 \mu\text{M}$ NMDA²¹, but might be explained by high KA sensitivity throughout the CA1 and CA3 regions⁴⁰ and relevant differences in cellular systems. Whole-cell current-clamp recordings provided further insights, how differences in Ca^{2+} and K^+ handling observed in $\text{Slack}^{-/-}$ hippocampal neurons translate into altered vulnerability to excitatory stimuli and ultimately more severe seizures *in vivo*. First, amplitudes of TTX-sensitive transient inward currents induced by depolarizing voltage steps were higher in $\text{Slack}^{-/-}$ neurons. At the same time, steady-state currents at membrane voltages between -20 to $+20$ mV were inward-directed indicating the presence of increased I_{NaP} that were previously reported for *Drosophila* neurons deficient in the Slack analogue Slo2⁴³ as well as in mammalian neurons^{11,17}. Additionally, decreased I_{NaP} was reported in GABAergic cortical neurons of mice carrying a Slack GOF variant⁴⁷, which is in line with our findings for Slack LOF neurons. Second, firing frequencies of AP trains induced by KA application or depolarizing current injection were significantly higher in $\text{Slack}^{-/-}$ than in controls (Fig. 6b, f). RMP (Fig. 6g), AP amplitude and aHP amplitudes (Fig. 6i and Supplementary Data 1) were not different between genotypes. While our findings on AP amplitudes are similar to data from dorsal root ganglia and glutamatergic neurons of the basolateral amygdala^{12,50}, those studies report slightly depolarized RMP. No altered RMP,

however, was reported for GABAergic and glutamatergic cortical neurons carrying a Slack GOF variant⁴⁷. These facts again underline that the impact of Slack channel function depends on the specific cellular system or tissue. Additionally, AP were elicited at more negative membrane voltages in $\text{Slack}^{-/-}$ (Fig. 6h) together with increased maximal AP rise slopes (Fig. 6k), indicating that increased net inward currents found in $\text{Slack}^{-/-}$ might influence discrete AP kinetics. Besides the raising phases of the AP, $\text{Slack}^{-/-}$ also display a shorter aHP (Fig. 6n). These findings are in line with findings in other models: $\text{Slack}^{-/-}$ dorsal root ganglion neurons show accelerated and deregulated firing patterns as well as increased AP rise slope and decreased AP threshold^{12,33}. Also, Slack-deficient glutamatergic neurons from the basolateral amygdala respond with increased AP firing rates to current injection while Slack GOF neurons respond with slower firing⁵⁰. The described reduction of the threshold depolarization necessary for eliciting AP might explain the increases in AP frequencies, Ca^{2+} influx and ultimately cell death as well as seizure severity observed in $\text{Slack}^{-/-}$. Accordingly, the absence of the Slack channel in genetically and pharmacologically induced epilepsy models of *Drosophila* promoted seizure-like neuronal activity. It was thus concluded that the repolarizing K^+ currents mediated by Slack serve as a protective brake against overexcitation⁴³. Combined with our current data we think that during depolarization, a Slack-mediated sustained K^+ outflow is involved in setting Na_V activation and thus AP threshold (Figs. 5c, 6n, and 6o). This subthreshold Slack current is probably activated by persistent sodium currents (Fig. 5d, e)¹⁷. In $\text{Slack}^{-/-}$, however, this Na_V activation brake is removed to allow Na_V activation and AP initiation at slightly more negative membrane potentials. This relative increase in depolarizing Na^+ currents would, in turn, allow

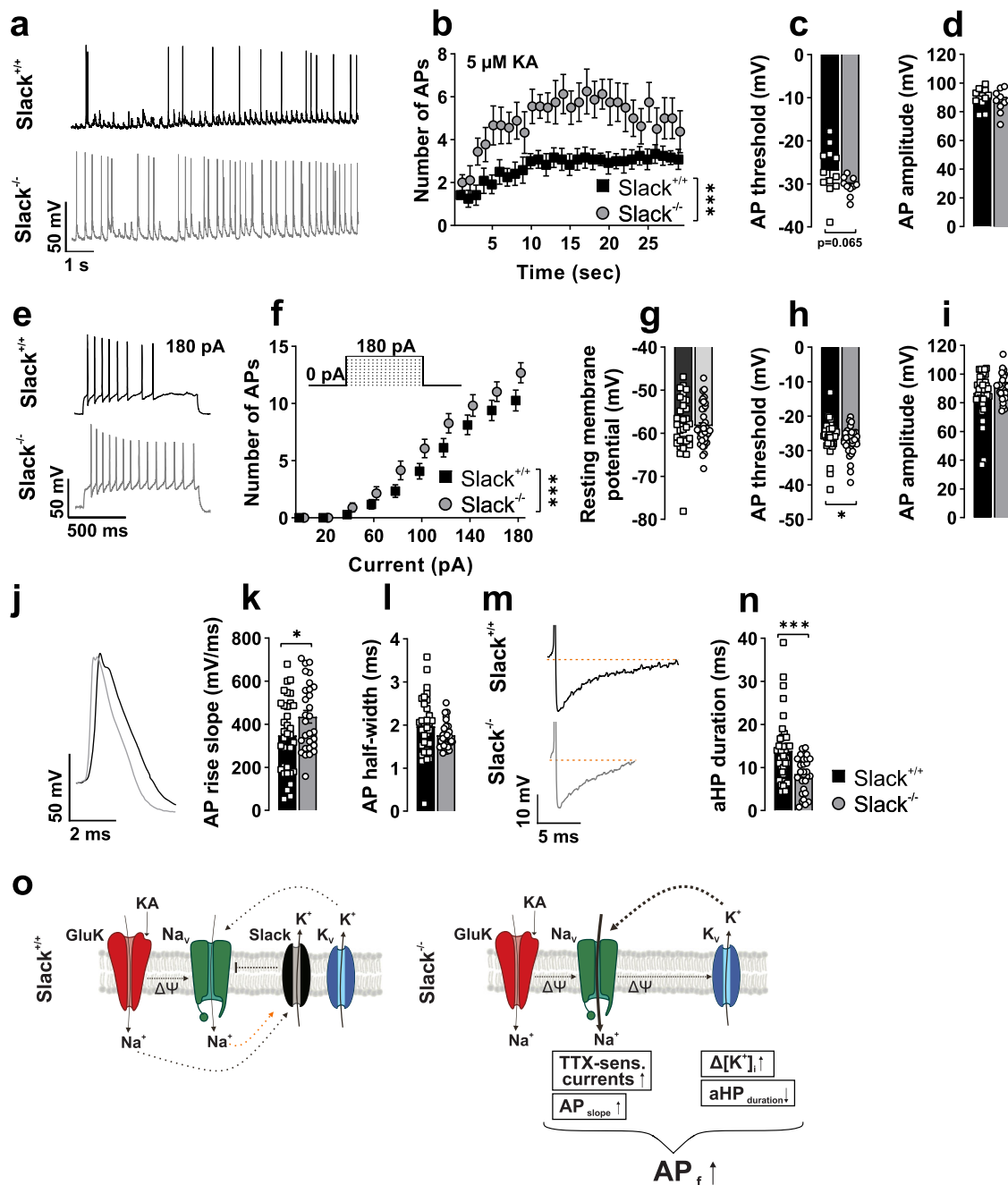


Fig. 6 Increased action potential frequencies in Slack^{-/-} hippocampal neurons. a-n Whole-cell current-clamp recordings from 14 div hippocampal neurons. **a** Representative current-clamp recordings from Slack^{+/+} and Slack^{-/-} neurons after application of 5 μ M KA. **b** Number of AP per 1 s bin after KA application was significantly (two-way ANOVA, $F_{1,551} = 175.4$, $p < 0.001$) increased in Slack^{-/-} ($n = 12$ independent experiments from a total of $n = 12$ neurons from 6 preparations) compared to Slack^{+/+} ($n = 9$ from 4 preparations), while **c** action potential (AP) threshold (Welch's corrected unpaired t-test) and **d** amplitude were not significantly different. **e** Representative current-clamp recordings from Slack^{+/+} (top) and Slack^{-/-} (bottom) neurons during 180 pA current injection. **f** AP frequency in response to incremental current injection was significantly (two-way ANOVA $F_{1,668} = 20.50$, $p < 0.001$) increased in Slack^{-/-} ($n = 33$ neurons obtained from 8 preparations) compared to Slack^{+/+} cells ($n = 38$ neurons obtained from nine preparations). **g** Resting membrane potential was not different between genotypes. **h**, **i** Slack^{-/-} neurons displayed significantly (Mann-Whitney test $p = 0.043$) more negative threshold potential for initiation of AP firing than Slack^{+/+} neurons together with similar AP amplitude. **j** Representative current-clamp recording illustrating different AP kinetics between Slack^{+/+} (black) and Slack^{-/-} (gray). **k** Maximal AP rise slope is significantly (Mann-Whitney test $p = 0.041$) steeper in Slack^{-/-} ($n = 29$) compared to Slack^{+/+} ($n = 34$), while **l** AP halfwidth is similar between genotypes. **m** Representative current-clamp recordings illustrating different AP afterhyperpolarization (aHP) between Slack^{+/+} (black) and Slack^{-/-} (gray). **n** aHP duration is significantly (Mann-Whitney test $p = 0.0009$) shorter in Slack^{-/-} than Slack^{+/+} neurons. **o** Schematic illustration of proposed Slack function during KA-induced neuronal activation in Slack^{+/+} (left) and Slack^{-/-} (right). Lack of subthreshold Slack activity leads to disinhibition of Na_v channels to reduce AP threshold, which, in turn, increases AP frequency and presumably boosts K_v channel activation. Data represented as mean \pm SEM with $p < 0.05$ and < 0.001 . For detailed statistics also consult Supplementary Data 1.

increased AP frequencies to ultimately boost $[Ca^{2+}]_i$ and neuronal demise. Additionally, facilitated depolarization could also increase activation of voltage-gated K^+ channels (K_V), explaining the increased $[K^+]_i$ after stimulation with KA (Fig. 4f) and also faster aHP that provides faster repolarization for subsequent AP (Fig. 6f, n, o). Several members of the K_V1 family, for example, are activated between -20 and -30 mV of membrane depolarization and could thereby affect AP frequencies⁵¹.

We identified the following limitations of our study: (1) This study exclusively used male mice for in vivo experiments. Our findings might therefore not be transferable to female subjects. (2) Slack^{-/-} animals carry a global Slack deletion. Hence, alterations in brain development²² and compensatory regulations of other channels cannot be excluded. (3) The hippocampal formation is known to be tightly linked to epileptogenesis⁵² and is heavily affected by seizures⁵³. The KA-based model was reported to induce highly isomorphic seizures and hippocampal sclerosis-like damage in mice⁴⁰. However, a direct link to Slack-related epilepsies that are characterized and studied on a cortical level and seizures frequently located in the frontal cortex^{47,54} is somewhat limited. (4) Impact of seizures was analyzed 24 h after KA injection on mRNA level. Whether posttranslational modifications and compensation on a protein level in response to loss of Slack affect long-term outcomes is not reported here. (5) Further work on additional brain regions, with differentiation between excitatory and inhibitory neurons combining, for instance, conditional Slack knockout models and analysis of seizure-induced subcellular protein expression might complete our findings. (6) Voltage-clamp recordings were conducted to observe altered Na^+ -dependent K^+ currents. Due to the chosen experimental conditions, we cannot draw any conclusions about whether other conductances, e.g., voltage-gated Na^+ or Ca^{2+} channels are changed in Slack^{-/-}.

Taken together, our data imply that neuronal Slack activity needs to be tightly balanced, as excessive, and insufficient Slack function is detrimental depending on the cell types, tissues, and the factors triggering neuronal activity involved. In our study, increased excitability offers an explanation for severe seizures in a Slack LOF mutation³². It also urges caution when aiming for full Slack inhibition to treat GOF variant-induced epilepsies. It might be necessary to either develop partial Slack antagonists and/or to deliberate dosage, as too little Slack activity might well increase seizure susceptibility.

Data availability

This study includes no data deposited in external repositories. Source data underlying figures are provided in Supplementary Data 1. Further information and requests for source data should be directed to and will be fulfilled by the Lead Contact, Robert Lukowski (robert.lukowski@uni-tuebingen.de).

Received: 16 March 2023; Accepted: 25 September 2023;

Published online: 11 October 2023

References

- Brown, M. R. et al. Amino-termini isoforms of the Slack K^+ channel, regulated by alternative promoters, differentially modulate rhythmic firing and adaptation. *J. Physiol.* **586**, 5161–5179 (2008).
- Bhattacharjee, A., Gan, L. & Kaczmarek, L. K. Localization of the Slack potassium channel in the rat central nervous system. *J. Comp. Neurol.* **454**, 241–254 (2002).
- Rizzi, S., Knaus, H. G. & Schwarzer, C. Differential distribution of the sodium-activated potassium channels slick and slack in mouse brain. *J. Comp. Neurol.* **524**, 2093–2116 (2016).
- Kameyama, M., Kakei, M., Sato, R., Shibusaki, T., Matsuda, H. & Irisawa, H. Intracellular Na^+ activates a K^+ channel in mammalian cardiac cells. *Nature* **309**, 354–356 (1984).
- Wallen, P. et al. Sodium-dependent potassium channels of a Slack-like subtype contribute to the slow afterhyperpolarization in lamprey spinal neurons. *J. Physiol.* **585**, 75–90 (2007).
- Kim, U. & McCormick, D. A. Functional and ionic properties of a slow afterhyperpolarization in ferret perigeniculate neurons *in vitro*. *J. Neurophysiol.* **80**, 1222–1235 (1998).
- Yang, B., Desai, R. & Kaczmarek, L. K. Slack and Slick $K(Na)$ channels regulate the accuracy of timing of auditory neurons. *J. Neurosci.* **27**, 2617–2627 (2007).
- Kaczmarek, L. K. Slack, slick and sodium-activated potassium channels. *ISRN Neurosci.* **2013** (2013). <https://doi.org/10.1155/2013/354262>
- Franceschetti, S. et al. Na^+ -activated K^+ current contributes to postexcitatory hyperpolarization in neocortical intrinsically bursting neurons. *J. Neurophysiol.* **89**, 2101–2111 (2003).
- Liu, X. & Stan Leung, L. Sodium-activated potassium conductance participates in the depolarizing afterpotential following a single action potential in rat hippocampal CA1 pyramidal cells. *Brain Res.* **1023**, 185–192 (2004).
- Hage, T. A. & Salkoff, L. Sodium-activated potassium channels are functionally coupled to persistent sodium currents. *J. Neurosci.* **32**, 2714–2721 (2012).
- Martinez-Espinosa, P. L. et al. Knockout of Slo2.2 enhances itch, abolishes KNa current, and increases action potential firing frequency in DRG neurons. *Elife* **4**, 1–27 (2015).
- Reijntjes, D. O. J. et al. Sodium-activated potassium channels shape peripheral auditory function and activity of the primary auditory neurons in mice. *Sci. Rep.* **9**, 2573 (2019).
- Bhattacharjee, A. & Kaczmarek, L. K. For K^+ channels, Na^+ is the new Ca^{2+} . *Trends Neurosci.* **28**, 422–428 (2005).
- Bhattacharjee, A., Joiner, W. J., Wu, M., Yang, Y., Sigworth, F. J. & Kaczmarek, L. K. Slick (Slo2.1), a rapidly-gating sodium-activated potassium channel inhibited by ATP. *J. Neurosci.* **23**, 11681–11691 (2003).
- Yuan, A. et al. The sodium-activated potassium channel is encoded by a member of the Slo gene family. *Neuron* **37**, 765–773 (2003).
- Budelli, G. et al. Na^+ -activated K^+ channels express a large delayed outward current in neurons during normal physiology. *Nat. Neurosci.* **12**, 745–750 (2009).
- Nanou, E. & El Manira, A. A postsynaptic negative feedback mediated by coupling between AMPA receptors and Na^+ -activated K^+ channels in spinal cord neurones. *Eur. J. Neurosci.* **25**, 445–450 (2007).
- Nanou, E., Kyriakatos, A., Bhattacharjee, A., Kaczmarek, L. K., Paratcha, G. & El Manira, A. Na^+ -mediated coupling between AMPA receptors and KNa channels shapes synaptic transmission. *Proc. Natl. Acad. Sci. USA* **105**, 20941–20946 (2008).
- Uchino, S. et al. Slo2 sodium-activated K^+ channels bind to the PDZ domain of PSD-95. *Biochem. Biophys. Res. Commun.* **310**, 1140–1147 (2003).
- Ehinger, R. et al. Slack $K(+)$ channels attenuate NMDA-induced excitotoxic brain damage and neuronal cell death. *FASEB J.* **35**, e21568 (2021).
- Matt, L. et al. The $Na(+)$ -activated $K(+)$ channel Slack contributes to synaptic development and plasticity. *Cell Mol. Life Sci.* **78**, 7569–7587 (2021).
- Heron, S. E. et al. Missense mutations in the sodium-gated potassium channel gene KCNT1 cause severe autosomal dominant nocturnal frontal lobe epilepsy. *Nat. Genet.* **44**, 1188–1190 (2012).
- Barcia, G. et al. De novo gain-of-function KCNT1 channel mutations cause malignant migrating partial seizures of infancy. *Nat. Genet.* **44**, 1255–1259 (2012).
- Bonardi, C. M. et al. KCNT1-related epilepsies and epileptic encephalopathies: phenotypic and mutational spectrum. *Brain* **144**, 3635–3650 (2021).
- Aminkeng, F. KCNT1 mutations in ADNFLE and MMPSI: a new driver in the etiology and pathophysiology of early-onset epileptic syndromes. *Clin. Genet.* **83**, 319–320 (2013).
- Lim, C. X., Ricos, M. G., Dibbens, L. M. & Heron, S. E. KCNT1 mutations in seizure disorders: the phenotypic spectrum and functional effects. *J. Med. Genet.* **53**, 217–225 (2016).
- Tang, Q. Y. et al. Epilepsy-related slack channel mutants lead to channel overactivity by two different mechanisms. *Cell Rep.* **14**, 129–139 (2016).
- Kim, G. E. & Kaczmarek, L. K. Emerging role of the KCNT1 Slack channel in intellectual disability. *Front. Cell Neurosci.* **8**, 209 (2014).
- McTague, A. et al. Clinical and molecular characterization of KCNT1-related severe early-onset epilepsy. *Neurology* **90**, e55–e66 (2018).
- Vanderver, A. et al. Identification of a novel de novo p.Phe932Ile KCNT1 mutation in a patient with leukoencephalopathy and severe epilepsy. *Pediatr. Neurol.* **50**, 112–114 (2014).
- Evely, K. M., Pryce, K. D. & Bhattacharjee, A. The Phe932Ile mutation in KCNT1 channels associated with severe epilepsy, delayed myelination and leukoencephalopathy produces a loss-of-function channel phenotype. *Neuroscience* **351**, 65–70 (2017).
- Lu, R. et al. Slack channels expressed in sensory neurons control neuropathic pain in mice. *J. Neurosci.* **35**, 1125–1135 (2015).
- Happ, D. F. & Tasker, R. A. A method for objectively quantifying propidium iodide exclusion in organotypic hippocampal slice cultures. *J. Neurosci. Methods* **269**, 1–5 (2016).

35. Schindelin, J. et al. Fiji: an open-source platform for biological-image analysis. *Nat. Methods* **9**, 676–682 (2012).
36. Bischof, H. et al. Novel genetically encoded fluorescent probes enable real-time detection of potassium in vitro and in vivo. *Nat. Commun.* **8**, 1422 (2017).
37. Fourcaud-Trocme, N., Zbili, M., Duchamp-Viret, P. & Kuczewski, N. Afterhyperpolarization promotes the firing of mitral cells through a voltage-dependent modification of action potential threshold. *eNeuro* **9**, 1–21 (2022).
38. Swinscow, T. D. V. & Campbell, M. J. Statistics at square one. (Bmj London, 2002).
39. Sendrowski, K. & Sobaniec, W. Hippocampus, hippocampal sclerosis and epilepsy. *Pharm. Rep.* **65**, 555–565 (2013).
40. Levesque, M. & Avoli, M. The kainic acid model of temporal lobe epilepsy. *Neurosci. Biobehav. Rev.* **37**, 2887–2899 (2013).
41. Rusina, E., Bernard, C. & Williamson, A. The kainic acid models of temporal lobe epilepsy. *eNeuro* **8** <https://doi.org/10.1523/ENEURO.0337-20.2021> (2021).
42. Holopainen, I. E. Organotypic hippocampal slice cultures: a model system to study basic cellular and molecular mechanisms of neuronal cell death, neuroprotection, and synaptic plasticity. *Neurochem. Res.* **30**, 1521–1528 (2005).
43. Byers, N., Hahm, E. T. & Tsunoda, S. Slo2/K(Na) channels in drosophila protect against spontaneous and induced seizure-like behavior associated with an increased persistent Na(+) current. *J. Neurosci.* **41**, 9047–9063 (2021).
44. Quraishi, I. H. et al. Impaired motor skill learning and altered seizure susceptibility in mice with loss or gain of function of the Kcnt1 gene encoding Slack (K(Na)1.1) Na(+)–activated K(+) channels. *Sci. Rep.* **10**, 3213 (2020).
45. Igelstrom, K. M. Is slack an intrinsic seizure terminator? *Neuroscientist* **19**, 248–254 (2013).
46. Gertler, T. S., Cherian, S., DeKeyser, J. M., Kearney, J. A. & George, A. L. Jr K(Na)1.1 gain-of-function preferentially dampens excitability of murine parvalbumin-positive interneurons. *Neurobiol. Dis.* **168**, 105713 (2022).
47. Shore, A. N. et al. Reduced GABAergic neuron excitability, altered synaptic connectivity, and seizures in a KCNT1 gain-of-function mouse model of childhood epilepsy. *Cell Rep.* **33**, 108303 (2020).
48. Oyrer, J., Maljevic, S., Scheffer, I. E., Berkovic, S. F., Petrou, S. & Reid, C. A. Ion channels in genetic epilepsy: from genes and mechanisms to disease-targeted therapies. *Pharm. Rev.* **70**, 142–173 (2018).
49. Villa, C. & Combi, R. Potassium channels and human epileptic phenotypes: an updated overview. *Front. Cell Neurosci.* **10**, 81 (2016).
50. Zhang, Q. et al. The slack channel regulates anxiety-like behaviors via basolateral amygdala glutamatergic projections to ventral hippocampus. *J. Neurosci.* **42**, 3049–3064 (2022).
51. Gutman, G. A. et al. International Union of Pharmacology. LIII. Nomenclature and molecular relationships of voltage-gated potassium channels. *Pharm. Rev.* **57**, 473–508 (2005).
52. Goldberg, E. M. & Coulter, D. A. Mechanisms of epileptogenesis: a convergence on neural circuit dysfunction. *Nat. Rev. Neurosci.* **14**, 337–349 (2013).
53. Ozuna, J. Seizure disorders and epilepsy. *Cold Spring Harb. Perspect. Med.* **5**, a022426 (2000).
54. Mikati, M. A. et al. Quinidine in the treatment of KCNT1-positive epilepsies. *Ann. Neurol.* **78**, 995–999 (2015).

Acknowledgements

This work was funded in parts by the *Deutsche Forschungsgemeinschaft* (DFG) with individual grants to P.R. and R.L. and by the “Dr. Robert Pfleger-Stiftung” to R.L. R.L., P.R., and T.P. are members of the GRK2381: “cGMP: From Bedside to Bench”, DFG grant number 335549539. H.B. is a fellow of the Austrian Science Fund (FWF) funded Erwin-Schrödinger-Program, project number J4457. The authors acknowledge support from the Open Access Publishing Fund of the University of Tübingen. We thank Clement Kabagema-Bilan and Michael Glaser for their excellent technical support.

Author contributions

D.S., H.B., R.E., L.M., and R.L. designed experiments, and D.S. performed experiments. D.S. and L.M. analyzed data. T.P., H.B., R.E., P.R., L.M., and R.L. contributed resources, materials, and protocols. P.R., L.M., and R.L. contributed to the discussions. D.S. and L.M. wrote the manuscript. D.S., L.M., and R.L. edited the manuscript. P.R. and R.L. obtained funding. L.M., R.E., and R.L. supervised the project. All authors approved the content and submission of the paper.

Funding

Open Access funding enabled and organized by Projekt DEAL.

Competing interests

The authors declare no competing interests.

Additional information

Supplementary information The online version contains supplementary material available at <https://doi.org/10.1038/s42003-023-05387-9>.

Correspondence and requests for materials should be addressed to Robert Lukowski.

Peer review information *Communications Biology* thanks Bing Zhang and the other, anonymous, reviewer(s) for their contribution to the peer review of this work. Primary Handling Editors: Eliana Scemes and George Inglis.

Reprints and permission information is available at <http://www.nature.com/reprints>

Publisher's note Springer Nature remains neutral with regard to jurisdictional claims in published maps and institutional affiliations.



Open Access This article is licensed under a Creative Commons Attribution 4.0 International License, which permits use, sharing, adaptation, distribution and reproduction in any medium or format, as long as you give appropriate credit to the original author(s) and the source, provide a link to the Creative Commons licence, and indicate if changes were made. The images or other third party material in this article are included in the article's Creative Commons licence, unless indicated otherwise in a credit line to the material. If material is not included in the article's Creative Commons licence and your intended use is not permitted by statutory regulation or exceeds the permitted use, you will need to obtain permission directly from the copyright holder. To view a copy of this licence, visit <http://creativecommons.org/licenses/by/4.0/>.

© The Author(s) 2023